Ethanol Dehydration in HZSM-5 Studied by Density Functional Theory: Evidence for a Concerted Process

ARTICLE *in* THE JOURNAL OF PHYSICAL CHEMISTRY A · MARCH 2015

Impact Factor: 2.69 · DOI: 10.1021/jp513024z · Source: PubMed

THE JOURNAL OF PHYSICAL CHEMISTRY A

Article

pubs.acs.org/JPCA

Ethanol Dehydration in HZSM-5 Studied by Density Functional Theory: Evidence for a Concerted Process

Seonah Kim,*[,†] David J. Robichaud,[†] Gregg T. Beckham,[†] Robert S. Paton,[‡] and Mark R. Nimlos*[,†]

[†]National Bioenergy Center, National Renewable Energy Laboratory, 15013 Denver West Parkway, Golden, Colorado 80401-3393, United States;

[‡]Chemistry Research Laboratory, Mansfield Road, Oxford OX1 3TA, United Kingdom

Supporting Information

ABSTRACT: Dehydration over acidic zeolites is an important reaction class for the upgrading of biomass pyrolysis vapors to hydrocarbon fuels or to precursors for myriad chemical products. Here, we examine the dehydration of ethanol at a Brønsted acid site, T12, found in HZSM-5 using density functional theory (DFT). The geometries of both cluster and mixed quantum mechanics/molecular mechanics (QM:MM) models are prepared from the ZSM-5 crystal structure. Comparisons between these models and different DFT methods are conducted to show similar results among the models and methods used. Inclusion of the full catalyst cavity through a QM:MM approach is found to be important, since activation barriers are computed on average as 7 kcal mol^{-1} lower than those obtained with a smaller cluster model. Two different pathways, concerted and stepwise, have been considered when examining dehydration and deprotonation steps. The current study shows that a concerted dehydration process is possible with a lower (4−5 kcal mol^{-1}) activation barrier while previous literature studies have focused on a stepwise mechanism. Overall, this work demonstrates that fairly high activation energies (~50 kcal mol^{-1}) are required for ethanol dehydration. A concerted mechanism is favored over a stepwise mechanism because charge separation in the transition state is minimized. QM:MM approaches appear to provide superior results to cluster calculations due to a more accurate representation of charges on framework oxygen atoms.

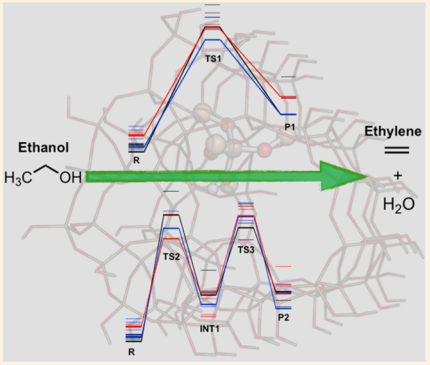

INTRODUCTION

Catalytic dehydration is a promising process for the conversion of bioethanol into ethylene,[1−5] which is a high volume feedstock for a wide range of chemicals and materials production. This reaction is also an important first step in the production of hydrocarbons or gasoline[2,3,6−11] from bioethanol. Finally, the dehydration of ethanol to ethylene is an important model reaction for studying dehydration occurring during the vapor phase upgrading of biomass pyrolysis vapors.[12,13] Thus, an understanding of the mechanism and kinetics of this simple reaction can have an important impact on many biofuels technologies.

Unimolecular dehydration of alcohols results from the elimination of the hydroxyl group and a hydrogen atom from an adjacent carbon resulting in the formation of an olefin. For instance, dehydration of ethanol would result in the formation of ethylene as shown in reaction 1. Dehydration reactions also occur as part of condensation reactions that are catalyzed by acid catalysts. For instance, the condensation of ketones results in the formation of alcohols, which are readily dehydrated. The most simple and perhaps most highly studied is acetone.[14−19] As shown in reaction 2, acetone will undergo aldol condensation on acid catalysts to form diacetone alcohol followed by dehydration to mesityl oxide. Dehydration reactions have fairly high reaction barriers and are typically considered rate-limiting reactions during coupling. For instance, aldol condensations in zeolites (HZSM-5 and HY) have a reaction barrier of about 20 kcal mol^{-1}, and the dehydration reaction will likely have a barrier of 40−50 kcal mol^{-1}.[20] Thus, dehydration is rate-limiting, and a thorough understanding of the mechanisms and energetics of dehydration is of great importance to developing improved catalysts.

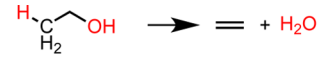

(1)

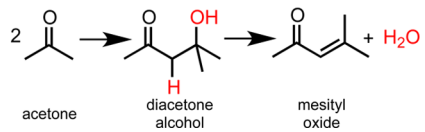

(2)

Ethanol is an ideal model alcohol for studying dehydration in acid catalysts. It is the smallest alcohol that will form an alkene upon dehydration and contains C−H, C−O, C−C, and O−H bonds found in biomass. As a result, detailed quantum mechanical studies are possible using accurate theoretical approaches. In addition, it is small enough to fit in the

Received: December 31, 2014
Revised: March 23, 2015
Published: March 24, 2015

DOI: 10.1021/jp513024z
J. Phys. Chem. A 2015, 119, 3604−3614

micropores of HZSM-5, which is the catalytic system examined here.

The unimolecular, uncatalyzed dehydration of ethanol produces ethylene and water through a 4-center transition structure (TS) as shown in mechanism 1. The reaction is endothermic, with an experimentally determined energy of reaction[21] of 11 kcal mol^{-1} and an activation energy of 72.0 kcal mol^{-1}.[22] Composite *ab initio* CBS-QB3 calculations[23] suggest addition of an alkali metal cation or a proton significantly lowers the dehydration barrier to 55.3 kcal mol^{-1} for ethanol clustered to Li^+ and to 20.7 kcal mol^{-1} for protonated ethanol.[23] The bimolecular dehydration of ethanol, in which a second ethanol molecule acts as a catalyst/proton shuttle, is similarly feasible (mechanism 2). The dehydration activation energy barrier and reaction energy were calculated (CBS-QB3) as 55.4 and 9.9 kcal mol^{-1}, respectively.

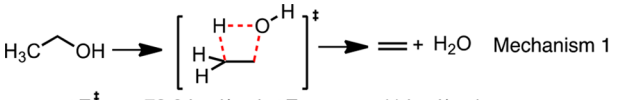

$\Delta E^{\ddagger}_{Exp.}$ = 72.0 kcal/mol, $\Delta E_{rxn, Exp.}$ = 11 kcal/mol

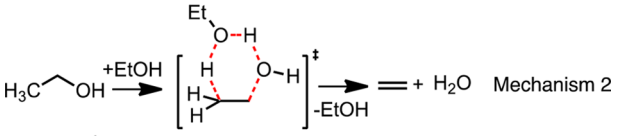

$\Delta E^{\ddagger}_{CBS\text{-}QB3}$ = 55.4 kcal/mol, $\Delta E_{rxn, CBS\text{-}QB3}$ = 9.9 kcal/mol

Zeolites are important materials in the dehydration of ethanol[1,5,24,25] and are also potential catalysts for upgrading biomass pyrolysis vapors.[26−29] In zeolites, Brønsted acid sites exist where framework silicon atoms are substituted with aluminum atoms. Perhaps one of the most commonly studied zeolites and one with the strongest measured acid sites[30,31] is HZSM-5, which has the MFI crystal structure.[32]

Brønsted acid sites in HZSM-5 provide a source of protons to catalyze unimolecular ethanol dehydration as illustrated in Schemes 1 and 2. As with the computational modeling of gas

Scheme 1. Proton Transfers in Ethanol Dehydration

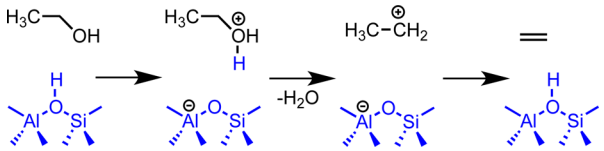

phase ethanol dehydration,[23] it has been proposed that the acidic proton transfers from the zeolite to the OH group on ethanol, which subsequently releases water to form an intermediate. This may be a carbocation or an alkoxide formed by coordination to a framework oxygen atom.[33,34] Deprotonation at the β-position transfers a proton back to the zeolite and completes the catalytic cycle as shown in Scheme 1.

Although an acidic proton is available, transfer of this proton to ethanol and subsequent dehydration of the protonated species may be problematic due to the high energetic cost of charge separation. In this study, we propose two alternative mechanisms (Scheme 2) that do not involve the formation of a free carbocation. These reaction mechanisms are possible because aluminum substitution in the silicon framework results in four nearly equivalent oxygen sites around the aluminum atom. In mechanism 3 (hereafter referred to as the "concerted mechanism"), proton transfers from the zeolite Brønsted acidic

Scheme 2. Two Proposed Mechanisms in Ethanol Dehydration: (a) Mechanism 3 (Concerted) and (b) Mechanism 4 (Stepwise)

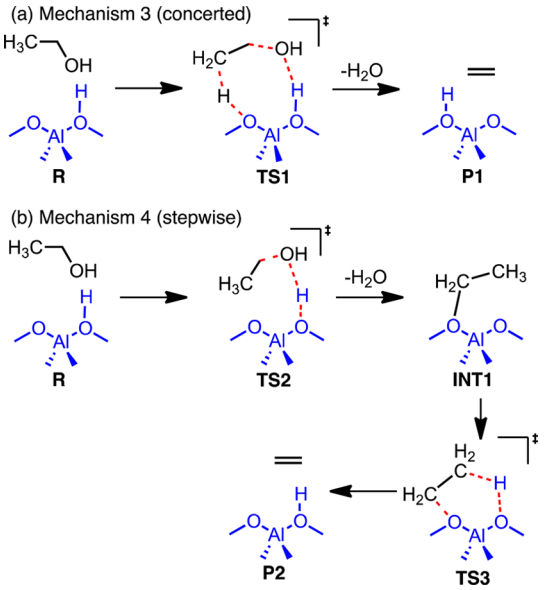

site (Al−(OH)−Si) to the alcohol are concurrent with water loss and a proton transfer from the C2 of ethanol to an adjacent partially negatively charged oxygen atom of the zeolite framework (Al−O−Si). Since there are eight atoms involved in this cyclic TS, the strain is much less than that in the four-center TS in mechanism 1. This type of ring strain reduction often results in a decrease in activation energy of 10−30 kcal mol^{-1}.[35,36] Thus, one might expect the barrier for this reaction to be 30−50 kcal mol^{-1}, based upon the gas phase barrier of 72.0 kcal mol^{-1}.[21,22] In mechanism 4 (hereafter referred to as the "stepwise mechanism"), proton transfer from Al(OH)Si to the alcohol occurs simultaneously with water loss and bonding of the α carbocation to Al−O−Si.[33,34,37] This reaction forms an ethyl group bound to the oxygen site. The ethyl group can transfer a proton from the β carbon to an adjacent Al−O−Si and form ethylene. TS1 in concerted mechanism will likely be more stable than TS2 in stepwise mechanism because the latter looks like a "frontside attack" (the attacking group approaches on the same side as the leaving group) S_N2/S_Ni mechanisms. The reaction barriers for the frontside attack are at least 2.4 kcal mol^{-1} higher compared to the backside attack.[38,39] Similar reaction mechanisms[40−44] involving oxygen atoms adjacent to the aluminum active site and concerted mechanisms have been proposed for a number of different types of reactions in zeolites, but we are unaware of reports of this type of mechanism for alcohol dehydration.

Density functional theory (DFT) has long been effectively used to study reaction mechanisms in the micropores of well-defined zeolites.[45−49] Typically, these calculations require approximations to make the calculations tractable. Two of the prominent finite-sized approaches are cluster calculations, in which only the active site is modeled, and mixed quantum mechanics/molecular mechanics (QM:MM) calculations such as ONIOM (our own *n*-layered integrated molecular orbital and molecular mechanics)[50] in which the active site is treated with a high level of theory and the remainder of the system is treated at a lower level of theory. However, the effectiveness of these two approaches is seldom compared. Fermann et al.

DOI: 10.1021/jp513024z
J. Phys. Chem. A 2015, 119, 3604−3614

compared constrained cluster (QM only) and embedded cluster (using ONIOM) calculations for proton transfer in H−Y zeolites.[51] By comparing the results for increasing cluster size, they determined that embedded cluster (ONIOM models) performed better than similar-sized constrained clusters (QM model). The embedded ONIOM models with smaller clusters converged reaction energies for the QM system with at least eight silicon or aluminum atoms. It should be pointed out that periodic boundary condition calculations are less frequently used to investigate reaction mechanisms in zeolites. Though perhaps more accurate than the finite-size models, these calculations are very time-consuming and are difficult to obtain transition state geometries and energies for all possible conformations.

In this study, we investigate the mechanisms, thermochemistry, and kinetics of ethanol dehydration at Brønsted acid sites in HZSM-5. The energetics and conformations of the reactions shown in Scheme 2 are investigated and compared for cluster and ONIOM models and for different DFT functionals and basis sets.

METHODS

We consider the dehydration of ethanol at the T12 site, when the silicon atom at this site is substituted with an aluminum atom. This is the most likely site for substitution during alumination of the silica framework.[52,53] The excess negative charge on the adjacent oxygen atoms can be balanced with a proton, creating a Brønsted acid site. Figure 1 shows a

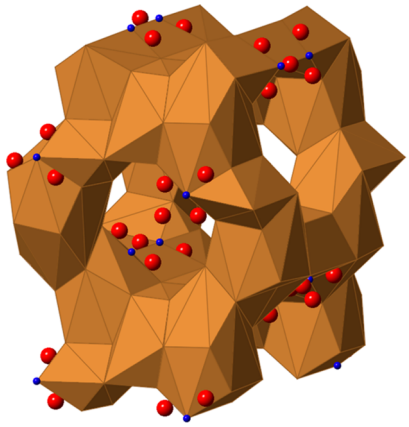

Figure 1. Scaled representation of the junction of HZSM-5. The blue spheres show the location of the T12 site, and the red spheres are the adjacent oxygen atoms.

representation of the intersection of the two microchannels in ZSM-5, where rings with fewer than six silicon atoms have been filled in. The blue spheres in this figure show the location of the T12 silicon atoms, and the red spheres show the location of the oxygen atoms adjacent to these silicon atoms. These oxygen atoms are the conjugate Brønsted acid sites, when the silicon atom at this site is substituted with an aluminum atom.

We have used two representations of the T12 site in HZSM-5: a quantum chemical cluster approach in which this site is modeled as an aluminum tetrasiloxide and an ONIOM treatment of a cluster embedded in the silica framework.[51] Two different partitions between the high level DFT and the low level semiempirical regions were examined using the ONIOM methodology. The three models, called cluster (Figure 2a), 5T ONIOM (Figure 2b), and 12T ONIOM (Figure 2c) models are shown in Figure 2.

Cluster Model. The cluster model (Figure 2a) contains a T12 atom and the four coordination spheres around it, which are terminated by SiH_3 groups with Si−H distance of 1.46 Å. The distance was determined from optimization of SiH_4 at the same level of theory. The H atoms were oriented toward the positions occupied in the crystal by the oxygen atoms in the next coordination sphere. Cartesian coordinates of SiH_3 groups were fixed during all geometry optimizations, thus retaining the crystallographic orientations. All of the calculations were performed using the hybrid meta generalized gradient approximation M06-2X functional[54] with the 6-311G(d,p) basis set. Through the inclusion of an electronic kinetic energy density term, this functional describes the effects of medium-range correlation important in the noncovalent interactions between the substrate and the zeolite.

ONIOM Model. All ONIOM model calculations were performed using the two-layer ONIOM scheme.[55] The high level DFT layer contains a 5T cluster (5T ONIOM model) or 12T cluster (12T ONIOM model) and one ethanol molecule. The DFT layer of the 5T ONIOM model contains the T12 atom (substituted by an Al atom), a Brønsted acid site proton, four coordination spheres around it, and ethanol, while the 12T ONIOM model has an additional 10-membered rings (10-MR) in the high layer. The semiempirical layer has all of the other 295 atoms as the low level (Figure 2b,c). One high level DFT functional and basis set are the same as that used in the cluster model (M06-2X/6-311G(d,p)), while the low level was treated with PM6.[56] As will be discussed, the 5T embedded cluster models produced energies that were nearly identical to the 12T embedded cluster models, and both models produced energies that were significantly different from the cluster models. This result is similar to what was found elsewhere,[51] and we thus selected the 5T ONIOM model for additional studies using other functionals, because results obtained using this model are converged with respect to the system size. One consideration of the use of the 5T ONIOM model is that the ethanol is forced into a geometry closer to the TS by the PM3-layer atoms. We saw no evidence of this when comparing our geometries to the 12T model or to a selected case of reactants using a 20T model. Using the 5T ONIOM model, calculations were also conducted with B3PW91/6-311G(d,p), B3LYP/6-311G(d,p), and M06-2X/6-31G(d) for the QM layer. All atoms in the DFT layer were allowed to relax freely, while the semiempirical layer atoms were restrained to maintain the crystallographic positions to capture the steric and electronic effects of the extended catalyst structure. Optimization of this outer region would introduce erroneous geometric effects associated with truncation of the periodic structure to a model cluster.

For both the cluster and the ONIOM models, vibrational frequency calculations were performed for all optimized structures to verify reactants, intermediates, products, and TSs. Intrinsic reaction coordinate (IRC) calculations were also performed for all transition structures both forward and reverse directions to determine two relevant minima.[54,57−60] Effects of the inclusion of an atom-pairwise density-independent London dispersion correction were examined with DFT-D3,[61] and results are shown in the Supporting Information (SI). All calculations were performed using the Gaussian 09 package.[62]

Naming Convention. In the discussion of the reactants, TSs, and intermediates in mechanisms 2 and 3, we adopt the following naming convention. The reactant configurations with

DOI: 10.1021/jp513024z
J. Phys. Chem. A 2015, 119, 3604−3614

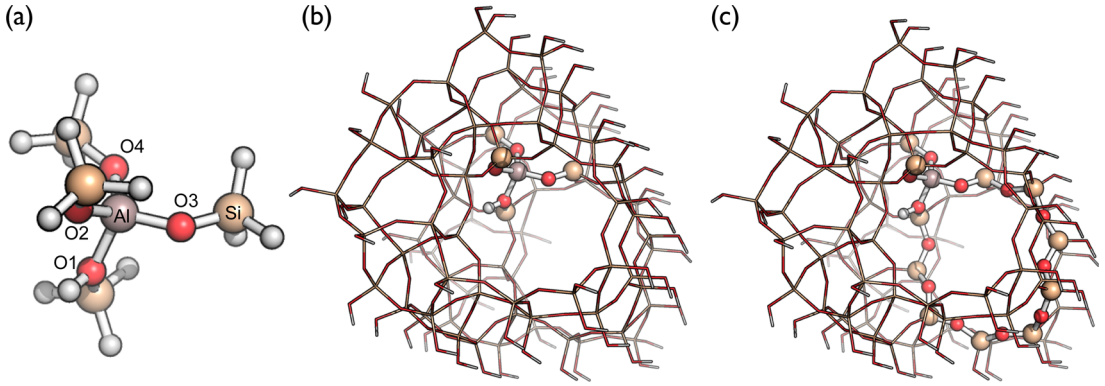

Figure 2. Three model systems: (a) Cluster model, where all atoms are treated using M06-2X/6-311G(d,p), (b) 5T ONIOM model, and (c) 12T ONIOM model. Atoms shown in ball and stick representation are treated with the M06-2X/6-311G(d,p) DFT model while the atoms shown by the wire frame were treated with PM6 in both 5T and 12T ONIOM models.

the ethanol hydrogen bonded to the Brønsted acid proton are given names such as $R1_{O1}$, where the O1 subscript indicates that the OH group on the ethanol is hydrogen bonded to the O1 sites as shown in Figure 3. The structures and energies of

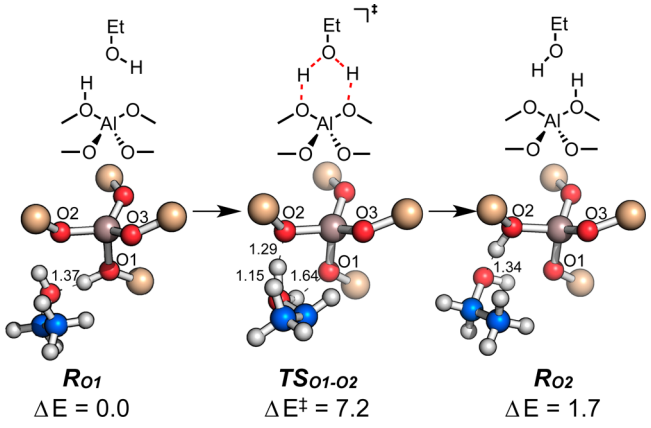

Figure 3. Calculated geometry transformations during the proton transfer path with ethanol from O1 to O2 position. M06-2X/6-311G(d,p):PM6 energies (kcal mol^{-1}) determined using the 5T ONIOM model. Atoms in the low-level region are not shown for visual clarity.

several conformers were calculated for hydrogen bonding to each proton site. The lowest energy reactant for site O1 is $R1_{O1}$, while the other conformers have names such as $R2_{O1}$. TSs are given names such as $TS1_{O1-O2}$, which is the TS number one as shown previously, where the subscripts indicate that the reaction involves sites O1 and O2. In this case, the proton is transferred from site O1 to site O2. Intermediates are named according to the site where the ethyl is bound, so $INT1_{O1}$ indicates that the ethyl is bound to the O1 site. Products are named according to the TS from which they originated, so $P1_{O1-O2}$ indicates the ethylene and water product from $TS1_{O1-O2}$.

RESULTS AND DISCUSSION

Brønsted Acid Sites. For the reactions at a Brønsted T12 site, there are four possible acid locations, which are the four oxygen atoms attached to the substituted aluminum. These are shown as O1−O4 in Figure 2. O4 was neglected because it is located within a small cavity defined by four- and six-membered rings that is unlikely to participate in the catalytic reactions. The O1, O2, and O3 sites are each capable of being a catalytically active Brønsted acid location, and the proximity of these locations allows for concerted reactions during dehydration, which lowers the reaction energy barriers.

A comparison of the calculated energies for the model systems with a proton at one of these Brønsted sites can provide an indication of the relative proton affinities and suggests the most likely location for reaction. Table 1 compares

Table 1. Relative[a] Energies (kcal mol^{-1}) of Models with the Proton Located at Different Sites

	cluster	5T ONIOM	12T ONIOM
O1	0.0	0.0	0.0
O2	1.3	1.7 (0.1−0.3)[b]	0.5
O3	3.9	6.2 (0.0002−0.02)[b]	7.3
O4	9.5	10.9 (10^{-7} − 0.0002)[b]	6.5

[a]Energies were determined using M06-2X/6-311G(d,p) or ONIOM-(M06-2X/6-311G(d,p):PM6) and are relative to a proton on the O1 site. [b]Boltzmann weighting for 100−500 °C.

the relative proton affinity for the different sites shown in Figure 2. As shown, protonation at O1 and O2 are close in energy and 4−10 kcal mol^{-1} more favorable than protonation at O3 or O4. Boltzmann weightings using the 5T ONIOM model are shown for 100−500 °C. As can be seen, even at high temperatures, the populations of O3 and O4 are less than 2%.

Interestingly, these calculations appear to be different from earlier correlations between the Al−O bond and the acid strength of the Si(OH)Al site. Earlier calculations[63] were conducted using a similar approach, where optimized 8T clusters were imbedded in frozen 30T−40T clusters. A correlation was observed between the length, the inverse of the strength of the Al−O bond, and the strength of the O−H bond. This was attributed to bond conservation,[64] with a weaker O−H bond corresponding to higher acidity. In the 5T model, the Al−O bond for sites O1 and O2 is 1.85 Å, while the bond is 1.89 Å for O3 and 1.90 Å for O4. Thus, the strength of the Al−O bond is higher upon protonation at O1 and O2 than O3 and O4. As can be seen in Table 1, the OH bond energy for O3 and O4 is about 4−10 kcal mol^{-1} greater compared to O1 and O2. No correlation was observed for the O−H bond

DOI: 10.1021/jp513024z
J. Phys. Chem. A 2015, 119, 3604−3614

strength as a function of the Al−O−Si angle, which is consistent with earlier calculations.[63]

The barriers to proton transfer between sites also affect the probability of the different Brønsted sites participating in dehydration. Figure 4 shows a plot of the potential energy for

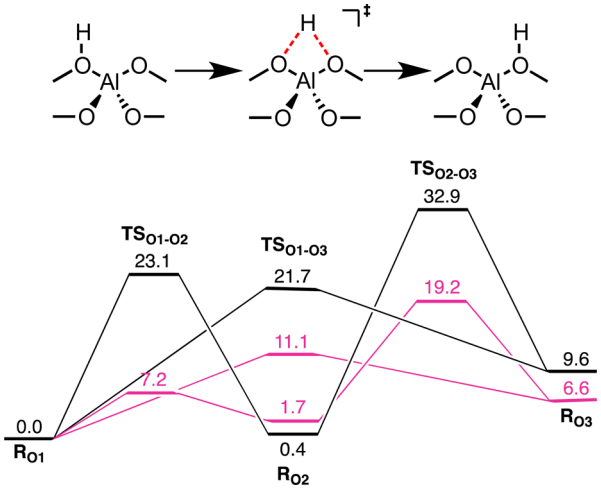

Figure 4. Reaction energy diagram of proton transfer among O1, O2, and O3 unassisted (in black) and shuttled by a molecule of ethanol (in pink). M06-2X/6-311G(d,p):PM6 energies (kcal mol^{-1}) determined using the 5T ONIOM model.

transferring between these sites using the 5T ONIOM model. The barriers for transferring a proton from one site to another are between 21.7 and 32.5 kcal mol^{-1}. These values are slightly higher than experimental measurements of 4−14 kcal mol^{-1}.[65,66] It has been suggested[45,51] that the presence of other molecules, such as water will lower the barrier for proton hopping and that this may explain the disparity between the calculated and measured values. In fact, these lower experimental barriers are consistent with calculated barriers for ethanol-assisted proton transfer, as discussed later.

Figure 4 also shows the relative energies for the transfer of a proton from one site to another facilitated by ethanol, acting as a proton shuttle. The barriers are lowered by nearly 50% (from 21.7−32.9 to 7.2−19.2 kcal mol^{-1} ranges), due to the reduced strain in the TS. Figure 3 shows the structures for the reactant, TS, and product from proton transfer from O1 to O2 involving an ethanol molecule. Our calculated barrier of 7.2 kcal mol^{-1} is similar to that found[45] using BH&HLYP with a cluster model with a barrier of 7.5 kcal mol^{-1}. The low barriers in O1 and O2 suggest that the dehydration reaction will most likely occur from the lower energy Brønsted sites, O1 or O2. Interestingly, because these sites are more stable as shown in Table 1, they are actually less acidic than the O3 or O4 sites. As we will show, in spite of their lower acidity, sites O1 and O2 have lower reaction barriers for concerted dehydration of ethanol than site O3.

Binding of Ethanol. There are numerous conformations for the binding of ethanol to the T12 site. In this study, we only considered conformations in which the Brønsted acidic proton is hydrogen bonded to the oxygen atom on the ethanol. With this restriction, there is still a large number of conformers possible. There is a subset of these conformers in which the hydrogen atom of the alcohol group is hydrogen bonded to an adjacent oxygen site around the aluminum atom at the T12 site. These doubly hydrogen bonded conformers are about 5−10 kcal mol^{-1} lower in energy than the structures with a single hydrogen bond. For example, a double hydrogen bonded conformer (R1$_{O1}$) is 4.6 kcal mol^{-1} lower in energy than one hydrogen bonded (R11$_{O1}$) in Figure 5. The lowest energy

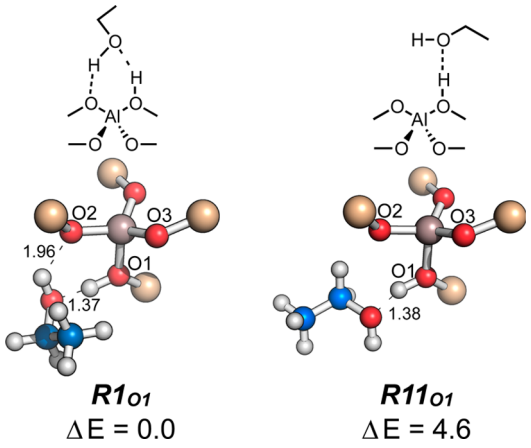

Figure 5. Geometry comparisons of one or double hydrogen bonded conformers (5T ONIOM model).

conformation found was a structure with the Brønsted acidic proton on O1, hydrogen bonded to the oxygen atom on the ethanol (1.37 Å) and the hydroxyl group weakly hydrogen bonded to O2 (1.96 Å) shown in Figure 5 (R1$_{O1}$). The relative energies for ethanol binding to protons on the O1, O2, and O3 sites are roughly equal to the relative energies of these sites without ethanol as shown in Table 1 and are collected in Table S1 in the SI.

Comparison of Computational Models. The two dehydration reaction pathways shown in mechanisms 3 and 4 earlier were considered in this study. For these reactions, two general pathways are possible for each protonated site, O1−O3 for six total possible pathways. For example, protonation at the O1 site can undergo the single step dehydration mechanism 3 to produce ethylene and water with a proton on O2 or O3. We calculated the energies of the starting configurations, TSs, and products for all six of these conformations using the three model systems discussed earlier. All of these calculations were conducted using M06-2X/6-311G(d,p) for high level and PM6 for low level. Figure 6 shows a comparison of the calculated energies of the reactants, TSs, and the products. The energies in these plots are relative to the energy for the lowest reactant conformation, R1$_{O1}$. The lowest TS for each Brønsted acid site is shown by the dark lines, while the other conformations are shown with thinner lines.

A comparison of the TS energies for the different models is provided in Table 2. These are averages of the energy differences between models and theoretical approaches. As can be seen, the cluster models produce TS energies that are on average 6.8 kcal mol^{-1} higher than the 5T ONIOM models, while for the energies for the 12T ONIOM models are 1.5 kcal mol^{-1} lower than the 5T ONIOM models. The 1.5 kcal mol^{-1} differences between the 5T and 12T ONIOM models suggest convergence has been approached with respect to the system size. To further investigate this, we conducted calculations of this same reaction pathway using a 20T ONIOM model in which two 10-silicon rings surrounding the ethanol atom are treated with M06-2X/6-31G(d) shown in Figure S1 in the SI. SI Table S2 showed energies of some representative TSs of 20T

DOI: 10.1021/jp513024z
J. Phys. Chem. A 2015, 119, 3604−3614

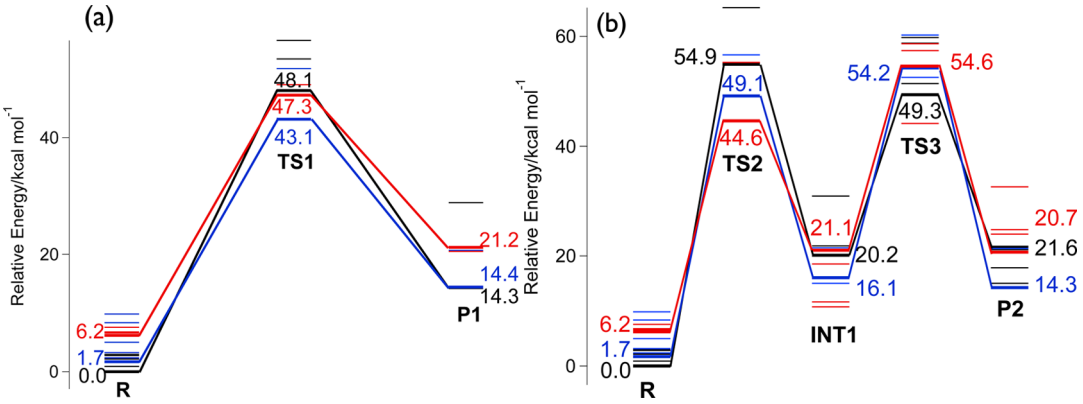

Figure 6. Reaction energy diagrams for (a) the concerted (mechanism 3) and (b) the stepwise (mechanism 4) reactions. The calculations were conducted using the 5T ONIOM (M06-2X/6-311G(d,p):PM6) model. The black symbols are for simulations started at the O1 site, the blue at the O2 site, and the red at the O3 site. The lowest energy pathway for each site is indicated by the lines connecting the points. The energy values shown are relative to the lowest reactant state for O1 ($R1_{O1}$).

Table 2. Comparison of Reaction Barriers Using Different Models and Theories

TS comparison[a]	avg. $\Delta\Delta E_{rel}$, kcal mol^{-1}
5T ONIOM: cluster[b]	−6.8 (5.7)
5T ONIOM: 12T ONIOM[b]	1.5 (3.2)
5T ONIOM models:	
M06-2X-B3LYP[c]	3.3 (3.5)
M06-2X-B3PW91[c]	1.1 (3.9)
M06-2X: 6-311G(d,p)-6-31G(d)[d]	−2.9 (0.6)

[a]Comparisons are made of the relative energies of the TSs for different models and theoretical approaches; i.e., $\Delta\Delta E_{rel} = \Delta E_{rel}$(5T ONIOM) − ΔE_{rel}(cluster). [b]Models are calculated using M06-2X/6-311G(d,p) for quantum calculations. [c]Using the 6-311G(d,p) basis set. [d]A comparison of different basis sets using the M06-2X DFT method. Standard deviations from all 25 TS conformations are shown in parentheses.

and 5T ONIOM models. Energy differences between these two ONIOM models are within 3 kcal mol^{-1}. These results support the notion that the large cluster limit has been reached with the 5T model. Adding more framework atoms to the quantum section does not appear to change the energetics significantly since we are investigating concerted reactions involving adjacent oxygen atoms attached to the Al atom.

The high TS energies calculated for the cluster calculations are a reflection of inaccuracies due to improper charge distribution in the framework. As can be seen in Table 2, the cluster barriers are on average 6.8 kcal mol^{-1} higher in energy than the 5T ONIOM calculations. This is not only due to the presence of Si−H bonds at the edge of the cluster model but also due to an incorrect polarization of the O−Si bonds. In particular we observe discrepancies in the computed atomic partial charges on the oxygen atoms around the aluminum atom at the T12 site between the cluster and larger model systems. For the ONIOM calculations, the Mulliken population charges on these atoms in the TS1, TS2, and TS3 are in the range −0.67 to −0.71 *e*, while the charge on these oxygen atoms in the cluster calculations is about −0.85 to −0.90 *e*. SI Table S3 shows the Mulliken charges for the 5T, 12T, and 20T ONIOM models for ethanol bound to site O1 and for the same structure using the cluster calculation. This charge discrepancy between the different models is likely due to the different abilities of σ^*_{Si-H} and σ^*_{Si-O} to accept electron density from the bonded oxygen atom. The SiH_3 group is a weaker acceptor than $Si(OR)_3$, so the oxygen atom in the cluster model contains an excess of negative charge in relation to the larger, more realistic model. Given that the formation of charged intermediates and TSs is prevalent to the chemistry occurring inside zeolites, this result cautions against the use of small cluster models in future work due to inaccuracies in the electrostatic potential that will inevitably result.

One might expect that the inaccuracy of the cluster calculations shown in Table 2 is due to the constraints placed upon the SiH_3 groups in the cluster models. However, inspection of the bond lengths, angles, and dihedral angles shows that the energy differences of the cluster calculations are not due to differences in flexibility. To see this, we focus on the calculated results for the most likely dehydration reaction, which is the concerted mechanism ($R1_{O1} \rightarrow TS1_{O1-O2} \rightarrow P1_{O2}$). It will be shown later that the concerted mechanism has the lowest calculated TS with proton being transferred from the O1 site and a proton being transferred from the ethanol to the O2 site. We extracted several bond lengths and angles from the protonated zeolite, reactants, and TSs for this reaction. The values are from the cluster and 5T and 12T ONIOM calculations and are collected in Table S4 in the SI. The root-mean-squared deviation (RMSD) of these bond lengths and angles and dihedral angles compared to the experimental zeolite structure without aluminum substitution are presented in Table 3. The RMSDs in all three cases are similar for each computational model. This suggests that in each model the

Table 3. RMSD of Bond Lengths (Å) and Angles (deg)

	cluster	5T ONIOM	12T ONIOM
Comparison of HZSM-5 to Neat ZSM-5			
bond lengths	0.28	0.31	0.31
angles	42	45	41
dihedral angles	21	25	20
Comparison of Ethanol Complex to Neat ZSM-5			
bond lengths	0.27	0.26	0.27
angles	31	41	38
dihedral angles	15	17	16
Comparison of TS to Neat ZSM-5			
bond lengths	0.22	0.24	0.25
angles	40	40	37
dihedral angles	27	28	26

DOI: 10.1021/jp513024z
J. Phys. Chem. A 2015, 119, 3604−3614

relaxation of the zeolite framework around the T12 site is similar and that this does not account for the observed relative energy differences between the TSs of the cluster model and the ONIOM models.

Another manifestation of this difference in charge distribution in the framework is the difference in the structure of the adsorbed ethanol substrate. To see this, we compare bond lengths and angles involving the reactant ethanol molecule and its TS. Several of the most critical values are collected in SI Table S5 for $R1_{O1}$ and $TS2_{O1-O2}$. Comparison bond lengths in $R1_{O1}$ show RMSD of 0.20 Å for the cluster model compared to the 12T ONIOM model while the RMSD is only 0.05 Å for the 5T ONIOM model compared to the 12T ONIOM model. Likewise the RMSDs for the angles are 18° and 3° for similar comparisons and 46° and 18° for the dihedrals. On the other hand, the RMSD comparison for $TS2_{O1-O2}$ shows that there is a little difference, 0.05 and 0.05 Å for bond lengths, 8.1° and 7.3° for angles, and 38° and 30° for dihedral angles. These values show that the difference in the TS energies for the cluster model is due to differences in the structure of the ethanol and its interaction with T12 catalyst site. It should be noted that for calculations where another layer of Si−O is added to the 5T model (a 17T model), the calculated RMSD are the same. This reduces the concern that the constraints on the ONIOM model systems lead to similar results.

Table 2 also compares different DFT functionals and the triple- and double-ζ basis sets. The average relative TS energies ($\Delta\Delta E_{rel}$) with B3LYP and B3PW91 functionals calculated 3.3 and 1.1 kcal mol^{-1}, respectively, lower than with M06-2X. B3LYP often underpredicts gas phase TSs by approximately 5 kcal mol^{-1}.[67−71] The 1.1 kcal mol^{-1} differences between B3PW91 and M06-2X suggest fair agreement, while the average difference between the triple- and double-ζ basis set is 2.9 kcal mol^{-1}. Full calculations to investigate basis set effects and other functionals including dispersion effects are summarized in Table S6 in the SI. In the remainder of this work, comparisons of reactions pathways will only be conducted using the 5T model.

Energetics of Reaction Pathways. The results of our calculations suggest that the concerted mechanism is slightly favored over the stepwise mechanism. All of the relative reaction energies including reactants, TSs , and products from mechanism 3 (Figure 6a) and mechanism 4 (Figure 6b) are shown in Figure 6 and are gathered in Table S1 in the SI together with the free energies. Values for the lowest energy pathways are indicated with the thicker lines and the diagonal lines connecting the TSs to the reactants, intermediates, and products. The color coding is for the different sites: black for O1, blue for O2, and red for O3. Averages for all of the calculated TSs are collected in Table 4. The free energies are obtained for the most stable conformers and also separately using the standard approach of a Boltzmann-weighted conformational ensemble which takes into account the contribution of all conformers to the partition function. These show that the average energies and free energies are roughly 4−5 kcal mol^{-1} lower in TS1 (concerted) than TS2 or TS3 (stepwise), while the standard deviation of the calculated values is 3−7 kcal mol^{-1}. The favored pathway is thus the concerted mechanism. As discussed earlier (Table 1), the Boltzmann factors favor the proton situated at the O1 site with a smaller probability at the O2 site. The lowest energy barriers for O1 and O2 sites are the concerted mechanisms with barriers (TS1) of 48.1 and 43.1 kcal mol^{-1}, while the first barriers

Table 4. Average Energies (kcal mol^{-1}) and Free Energies (kcal mol^{-1}) for TSs[a]

	5T ONIOM		12T ONIOM	
	ΔE_{rel}	ΔG_{rel}	ΔE_{rel}	ΔG_{rel}
TS1	50.2 (4.2)	46.2 (4.0)	50.2 (3.3)	46.0 (3.3)
TS2	54.3 (7.0)	51.7 (6.7)	54.9 (2.9)	52.2 (3.3)
TS3	53.7 (5.7)	49.5 (5.7)	51.0 (5.0)	46.9 (4.8)

[a]Energies are relative to the lowest energy state of ethanol bound to the proton on site O1. Averages are measured for the values shown in Supporting Information Table S1. Standard deviations of these values are shown in parentheses.

(TS2) for the stepwise mechanisms are 54.9 and 49.1 kcal mol^{-1} at the O1 and O2, respectively. A lower barrier is found for the stepwise mechanism for the O3 site, 44.6 kcal mol^{-1} compared to 47.3 kcal mol^{-1} from concerted, but the low population of this site suggests that this pathway is unlikely.

Given the small difference, one could say that the stepwise pathways are comparable, with the concerted mechanism slightly favored due to the limit of accuracy of the computational approach and conformational sampling. The higher energy of the stepwise mechanism can be understood in terms of the extent of charge separation. Figure 7 shows the molecular geometry with partial atomic charges by a Mulliken population analysis for concerted TS, $TS1_{O1-O2}$, which has a relative energy of ΔE_{rel} = 48.1 kcal mol^{-1} and the first stepwise TS, $TS2_{O1-O2}$, which has an energy of ΔE_{rel} = 54.9 kcal mol^{-1}. For $TS1_{O1-O2}$, the C_2H_2 fragment has a total Mulliken population charge of +0.767 *e* and the distance from the C_2H_2 fragment and the framework oxygen atom is about 2.70 Å. For $TS2_{O1-O2}$, the C_2H_3 fragment has a total Mulliken population charge of +0.966 *e* and is 2.59 Å from the framework oxygen atom. The charge separation for this primary carbocation increases the energy barrier of the stepwise mechanism relative to the concerted mechanism. One might expect that a secondary carbocation would be more stable and that the barrier for the stepwise mechanism of isopropyl alcohol ($CH_3CHOHCH_3$) would be lower. This is the focus of ongoing work in our group.

As mentioned previously, the reactant conformation with the lowest energy was $R1_{O1}$ in which the oxygen atom of the ethanol OH group was hydrogen bonded to the Brønsted acid proton and H on this group was hydrogen bonded to O3 (shown in Figure 5). All energies were relative to this state. This is shown as the thick black line on the left-hand side of the energy diagrams in Figure 6. The lowest energy conformations in the Brønsted acid proton on sites O2 and O3, $R1_{O2}$ and $R1_{O3}$, were 1.7 and 6.2 kcal mol^{-1} above $R1_{O1}$ which are shown in blue and red in Figure 6. The other conformations for the reactants were found by changing the hydrogen bonding partner of the H atom on the alcohol group or by rotating the ethyl group of ethanol about the C−O bond. The spread of energies for these conformers was typically low, about 3 kcal mol^{-1}.

The ethylene and water products from concerted mechanism were determined by following IRC calculations. No attempt was made to identify all of the conformations for these molecules, but significant variations in the energies were shown. This is largely due to the hydrogen bonding involving the water molecule. When the water is hydrogen bonded to the Brønsted acid proton and one of the other sites, the energies are low (~15 kcal mol^{-1}), while when the water only binds to a site, the energies are typically 20−25 kcal mol^{-1}. In Figure 8, water in

DOI: 10.1021/jp513024z
J. Phys. Chem. A 2015, 119, 3604−3614

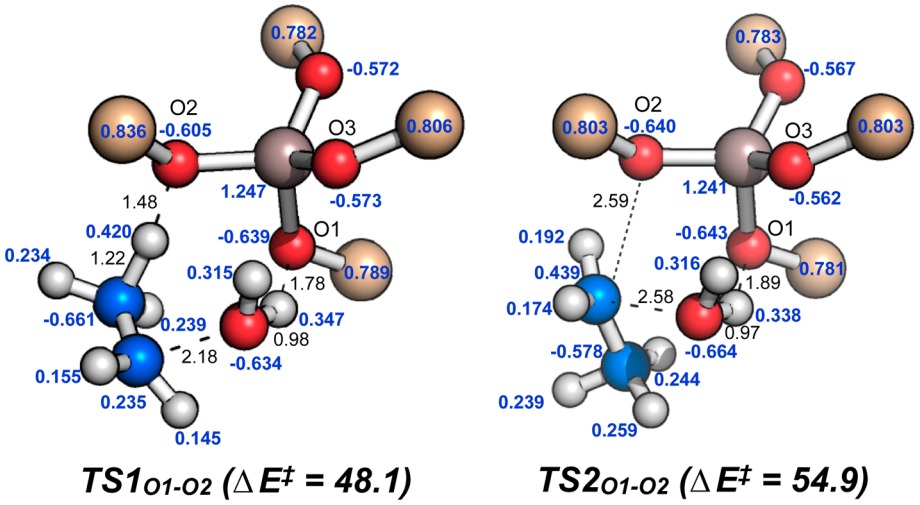

Figure 7. Optimized structures with bond distances (in black, Å) and Mulliken charges (in blue) for $TS1_{O1-O2}$ (left) and $TS2_{O1-O2}$ (right).

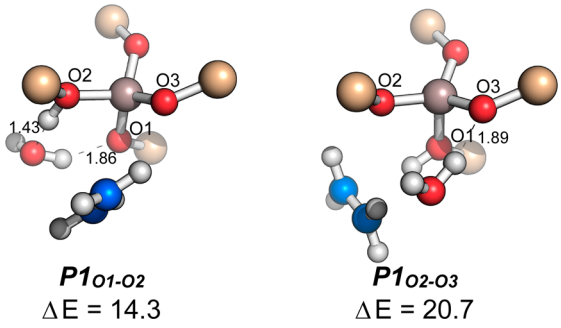

Figure 8. Geometry comparisons of a one or a two hydrogen bonded product.

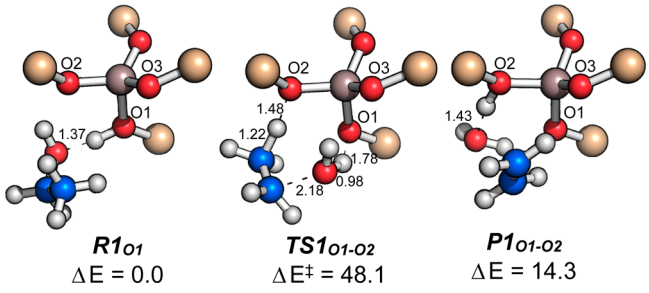

Figure 9. Geometry transformations during a concerted mechanism at the O1 position. Energies are given in kilocalories per mole calculated with 5T ONIOM calculation (M06-2X/6-311G(d,p):PM6). Bond distances are given in angstroms.

$P1_{O1-O2}$ has two hydrogen bonds between the oxygen atom of water and the Brønsted acid proton from the O2 framework and proton of water and O1 framework atom with ΔE = 14.3 kcal mol^{-1}, while $P1_{O2-O3}$ contains one hydrogen bond between the oxygen atom of water and the O3 framework atom with ΔE = 20.7 kcal mol^{-1}.

The intermediate conformations in the stepwise mechanisms were also determined by following IRC calculations to a minimum, and there was no attempt to identify all configurations. The energies of these molecules appear to be dependent upon the binding site. Binding of the ethyl group to O1 appears to have the lowest energy with an average of 12.1 kcal mol^{-1}, while the averages for O2 and O3 were 22.7 and 18.9 kcal mol^{-1}, respectively.

Structures of TSs. Figure 9 shows the important bond lengths for the concerted mechanism, the single step dehydration pathway ($R1_{O1} \rightarrow TS1_{O1-O2} \rightarrow P1_{O1-O2}$), and the corresponding bond lengths for all calculated TS1s are shown in Table S7 in the SI. In the transition state ($TS1_{O1-O2}$ in Figure 9), the bond length between the oxygen on the ethanol and the proton being transferred is R_{HO-H} = 0.98 Å, which is nearly the experimental O−H bond length for water, 0.95718 Å.[72] Further, the bond length between the O1 framework oxygen and the proton is R_{O-P} = 1.78 Å, and the C−O bond length in ethanol is R_{C-O} = 2.18 Å. These bond lengths indicate that an independent water molecule has formed at the TS. The bond length between O2 and the β proton is R_{O-H} = 1.48 Å and the β carbon and hydrogen of ethanol is R_{C-H} = 1.22 Å, showing the β proton is being transferred back to the O2 framework oxygen. For all of the TSs calculated for this mechanism there is a correlation between these two bond lengths and the calculated energy of the TS. The energy has a positive linear correlation with R_{C-H} with a coefficient of determination R^2 = 0.67 and R_{O-H} has a negative linear correlation with R^2 = 0.61. Thus, the closer the geometry of the TS is to the products, the higher the TS energy. The product of dehydration lies uphill in energy (shown in Figure 6), and therefore the TS lies closer in energy (and structure) to the product (Hammond−Leffler postulate). The imaginary frequency also has a positive correlation with R_{C-H} with R^2 = 0.97 and a negative correlation with R_{O-H} with R^2 = 0.94. As the TS moves closer to the products, the magnitude of the negative second derivative at the saddle point increases. The concerted mechanism indicates that, overall, the TS is "late" or close to the product structure. The acidic proton has completely transferred to the alcohol, the water molecule has dissociated, and the β proton is in the process of transferring to another oxygen site. To establish a quantitative correlation between the product and TS, the Brønsted−Evans−Polany reationship for the dehydration step has been considered and shows a correlation of R^2 = 0.52. This correlation is in the expected direction but is weaker than that found already for geometric parameters (e.g., the O−H distance in the computed TS structures) since all our energies are relative to $R1_{O1}$ only.

The TSs for the stepwise mechanism can also be considered "late" TSs. Figure 10 shows the TSs, intermediate, and product

DOI: 10.1021/jp513024z
J. Phys. Chem. A 2015, 119, 3604−3614

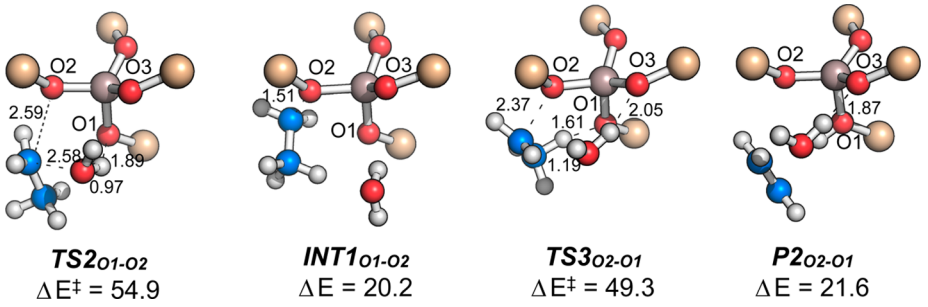

Figure 10. Geometry transformations during stepwise mechanism at the O1 position.

for the most likely reaction ($R1_{O1} \rightarrow TS2_{O1-O2} \rightarrow INT1_{O1-O2} \rightarrow TS3_{O2-O1} \rightarrow P2_{O2-O1}$), while all of the TSs are collected in SI Table S8 for TS2 and SI Table S9 for TS3. For $TS2_{O1-O2}$, the bond length from O1 to the proton is R_{O-P} = 1.89 Å, while the bond length from the ethanol oxygen atom to the proton is R_{HO-H} = 0.97 Å and the C−O bond length in ethanol is R_{C-O} = 2.58 Å. These bond lengths indicate that the proton has transferred to the oxygen atom on ethanol to form a water molecule. The ethyl group is also slowly transferring to the O2 site (R_{C-O2} = 2.59 Å). Thus, the bond lengths R_{C-O} and R_{C-O2} are important for this TS. These bond lengths are not correlated with the TS energy (R^2 = 0.22 and 0.13) while they are strongly negatively correlated to the imaginary frequency (R^2 = 0.92 and 0.80). The second TS ($TS3_{O2-O1}$) involving elimination of the ethyl group and transfer of hydrogen back to the O1 site shows also signs of being a late TS. The C−O bond between the ethyl group and O2 is 2.37 Å showing weak correlations between R_{C-O} and the TS energy (R^2 = 0.41), while dehydrated water is weakly hydrogen bonded to the O3 site of both $TS3_{O2-O1}$ and $P2_{O2-O1}$, 2.05 and 1.87 Å, respectively.

CONCLUSION

The DFT calculations conducted here show that ethanol dehydration in ZSM-5 can occur through cyclic TSs involving two framework oxygen atoms connected to the site of aluminum substitution. The Brønsted proton is transferred to the hydroxyl group of ethanol resulting in loss of water and formation of ethylene directly or an ethyl intermediate, which can then transfer a proton to form ethylene. The energies of the barriers for these two mechanisms are similar to the energies of about 50 and 54 kcal mol^{-1} for the concerted and stepwise mechanisms, respectively.

A comparison of computational approaches shows that ONIOM models produce reaction barrier energies that are on average about 7 kcal mol^{-1} lower than those obtained for cluster model. Increasing the size of the quantum layer for the ONIOM calculations beyond the 5T model does not significantly affect the barrier energies, and we propose that 5T ONIOM model is sufficient for these reactions.

ASSOCIATED CONTENT

Supporting Information

Tables listing relative and free energies, selected bond lengths and bond and dihedral angles, TS1 geometry of mechanism 2, TS2 and TS3 geometries of mechanism 3, and all optimized Cartesian coordinates for all calculations and a figure showing the 20T ONIOM model. This material is available free of charge via the Internet at http://pubs.acs.org.

AUTHOR INFORMATION

Corresponding Authors

*(S.K.) E-mail: seonah.kim@nrel.gov. Phone: 1-303-384-7323.
*(M.R.N.) E-mail: mark.nimlos@nrel.gov. Phone: 1-303-384-7704.

Notes

The authors declare no competing financial interest.

ACKNOWLEDGMENTS

This work was conducted as part of the Computational Pyrolysis Consortium supported by the U.S. Department of Energy's Bioenergy Technologies Office (DOE-BETO) Contract No. DE-AC36-08GO28308 with the National Renewable Energy Laboratory. Computer time was provided by the Texas Advanced Computing Center under the National Science Foundation Extreme Science and Engineering Discovery Environment Grant MCB-090159 and by the National Renewable Energy Laboratory Computational Sciences Center. R.S.P. acknowledges support from the SCG Innovation Fund (Catalysis in Confined Spaces).

REFERENCES

(1) Bi, J.; Guo, X.; Liu, M.; Wang, X. High Effective Dehydration of Bio-ethanol into Ethylene over Nanoscale HZSM-5 Zeolite Catalysts. *Catal. Today* **2010**, *149*, 143−147.
(2) Zhang, D.; Wang, R.; Yang, X. Effect of P Content on the Catalytic Performance of P-Modified HZSM-5 Catalysts in Dehydration of Ethanol to Ethylene. *Catal. Lett.* **2008**, *124*, 384−391.
(3) Madeira, F. F.; Gnep, N. S.; Magnoux, P.; Maury, S.; Cadran, N. Ethanol Transformation over HFAU, HBEA and HMFI Zeolites Presenting Similar Brønsted Acidity. *Appl. Catal., A* **2009**, *367*, 39−46.
(4) Phillips, C. B.; Datta, R. Production of Ethylene from Hydrous Ethanol on H-ZSM-5 under Mild Conditions. *Ind. Eng. Chem. Res.* **1997**, *36*, 4466−4475.
(5) Fan, D.; Dai, D.-J.; Wu, H.-S. Ethylene Formation by Catalytic Dehydration of Ethanol with Industrial Considerations. *Materials* **2013**, *6*, 101−115.
(6) Sousa, Z. S. B.; Cesar, D. V.; Henriques, C. A.; da Silva, V. T. Bioethanol Conversion into Hydrocarbons on HZSM-5 and HMCM-22 Zeolites: Use of in Situ DRIFTS to Elucidate the Role of the Acidity and of the Pore Structure over the Coke Formation and Product Distribution. *Catal. Today* **2014**, *234*, 182−191.
(7) Song, Z.; Takahashi, A.; Mimura, N.; Fujitani, T. Production of Propylene from Ethanol Over ZSM-5 Zeolites. *Catal. Lett.* **2009**, *131*, 364−369.
(8) Madeira, F. F.; Ben Tayeb, K.; Pinard, L.; Vezin, H.; Maury, S.; Cadran, N. Ethanol Transformation into Hydrocarbons on ZSM-5 Zeolites: Influence of Si/Al ratio on Catalytic Performances and Deactivation Rate. Study of the Radical Species Role. *Appl. Catal., A* **2012**, *443*−*444*, 171−180.

DOI: 10.1021/jp513024z
J. Phys. Chem. A 2015, 119, 3604−3614

(9) Maihom, T.; Khongpracha, P.; Sirijaraensre, J.; Limtrakul, J. Mechanistic Studies on the Transformation of Ethanol into Ethene over Fe-ZSM-5 Zeolite. *ChemPhysChem* **2012**, *14*, 101−107.
(10) Aldridge, G. A.; Verykios, X. E. Recovery of Ethanol from Fermentation Broths by Catalytic Conversion to Gasoline. 2. Energy Analysis. *Ind. Eng. Chem. Res.* **1984**, *23*, 733−737.
(11) Whitcraft, D. R.; Verykios, X. E.; Mutharasan, R. Recovery of Ethanol from Fermentation Broths by Catalytic Conversion to Gasoline. *Ind. Eng. Chem. Process Des. Dev.* **1983**, *22*, 452−457.
(12) Talmadge, M. S.; Baldwin, R. M.; Biddy, M. J.; McCormick, R. L.; Beckham, G. T.; Ferguson, G. A.; Czernik, S.; Magrini-Bair, K. A.; Foust, T. D.; Metelski, P. D.; et al. A Perspective on Oxygenated Species in the Refinery Integration of Pyrolysis Oil. *Green Chem.* **2014**, *16*, 407−453.
(13) Czernik, S.; Bridgwater, A. V. Overview of Applications of Biomass Fast Pyrolysis Oil. *Energy Fuels* **2004**, *18*, 590−598 c.
(14) Salvapati, G. S.; Ramanamurty, K. V.; Janardanarao, M. Selective Catalytic Self-Condensation of Acetone. *J. Mol. Catal.* **1989**, *54*, 9−30.
(15) Bosáček, V.; Kubelkova, L.; Novakova, J. Contribution of ^{13}C NMR Spectroscopy to the Analysis of Surface Compounds Formed in the Transformation of Acetone on Zeolites. *Catalysis and Adsorption by Zeolites*; Ohlmann, G., Pfeifer, H., Fricke, R. , Eds.; Elsevier: Amsterdam, 1991; Vol. *65*, pp 337−346.
(16) Hutchings, G. J.; Johnston, P.; Lee, D. F.; Warwick, A.; Williams, C. D.; Wilkinson, M. The Conversion of Methanol and Other O-Compounds to Hydrocarbons over Zeolite *β*. *J. Catal.* **1994**, *147*, 177−185.
(17) Panov, A. G.; Fripiat, J. J. Acetone Condensation Reaction on Acid Catalysts. *J. Catal.* **1998**, *178*, 188−197.
(18) Ramanamurty, K. V.; Salvapathi, G. S. Catalytic Cyclo-condensation of Acetone to Isophorone. *Indian J. Chem., Sect. B: Org. Chem. Incl. Med. Chem.* **1999**, *38*, 24−28.
(19) Tago, T.; Konno, H.; Sakamoto, M.; Nakasaka, Y.; Masuda, T. Selective Synthesis for Light Olefins from Acetone over ZSM-5 Zeolites with Nano- and Macro-crystal Sizes. *Appl. Catal., A* **2011**, *403*, 183−191.
(20) Migues, A. N.; Vaitheeswaran, S.; Auerbach, S. M. Density Functional Theory Study of Mixed Aldol Condensation Catalyzed by Acidic Zeolites HZSM-5 and HY. *J. Phys. Chem. C* **2014**, *118*, 20283−20290.
(21) Wiberg, K. B.; Hao, S. Enthalpies of Hydration of Alkenes. 4. Formation of Acyclic Tert-Alcohols. *J. Org. Chem.* **1991**, *56*, 5108−5110.
(22) Sivaramakrishnan, R.; Su, M. C.; Michael, J. V.; Klippenstein, S. J.; Harding, L. B.; Ruscic, B. Rate Constants for the Thermal Decomposition of Ethanol and Its Bimolecular Reactions with OH and D: Reflected Shock Tube and Theoretical Studies. *J. Phys. Chem. A* **2010**, *114*, 9425−9439.
(23) Nimlos, M.; Blanksby, S.; Ellison, G.; Evans, R. Enhancement of 1, 2-Dehydration of Alcohols by Alkali Cations and Protons: A Model for Dehydration of Carbohydrates. *J. Anal. Appl. Pyrolysis* **2003**, *66*, 3−27.
(24) Barthos, R.; Széchenyi, A.; Solymosi, F. Decomposition and Aromatization of Ethanol on ZSM-Based Catalysts. *J. Phys. Chem. B* **2006**, *110*, 21816−21825.
(25) Gayubo, A. G.; Tarrío, A. M.; Aguayo, A. T.; Olazar, M.; Bilbao, J. Kinetic Modelling of the Transformation of Aqueous Ethanol into Hydrocarbons on a HZSM-5 Zeolite. *Ind. Eng. Chem. Res.* **2001**, *40*, 3467−3474.
(26) Dickerson, T.; Soria, J. Catalytic Fast Pyrolysis: A Review. *Energies* **2013**, *6*, 514−538.
(27) Diebold, J.; Scahill, J. W. Biomass to Gasoline: Upgrading Pyrolysis Vapors to Aromatic Gasoline with Zeolite Catalysis at Atmospheric Pressure. *Pyrolysis Oils from Biomass: Producing, Analyzing, and Upgrading*, ACS Symposium Series; American Chemical Society: Washington, DC, USA, 1988, Vol. *376*, Chapter 23, pp 264−276.
(28) Biddy, M.; Dutta, A.; Jones, S.; Meyer, A. *Ex-Situ* Catalytic Fast Pyrolysis Technology Pathway, Technical Report NREL/TP-5100-58050; Bioenergy Technologies Office, U.S. Department of Energy: Washington, DC, USA, 2013; pp 1−9.
(29) Biddy, M.; Dutta, A.; Jones, S.; Meyer, A. *In-Situ* Catalytic Fast Pyrolysis Technology Pathway, NREL/TP, 5100-58056; 2013; pp 1−9.
(30) Suzuki, K.; Sastre, G.; Katada, N.; Niwa, M. Periodic DFT Calculation of the Energy of Ammonia Adsorption on Zeolite Bronsted Acid Sites to Support the Ammonia IRMS-TPD Experiment. *Chem. Lett.* **2009**, *38*, 354−355.
(31) Suzuki, K.; Sastre, G.; Katada, N.; Niwa, M. Quantitative Measurements of Brønsted Acidity of Zeolites by Ammonia IRMS-TPD Method and Density Functional Calculation. *Chem. Lett.* **2007**, *36*, 1034−1035.
(32) Olson, D. H.; Kokotailo, G. T.; Lawton, S. L.; Meier, W. M. Crystal Structure and Structure-Related Properties of ZSM-5. *J. Phys. Chem.* **1981**, *85*, 2238−2243 (Database of Zeolite Structures).
(33) Kondo, J. N.; Nishioka, D.; Yamazaki, H.; Kubota, J.; Domen, K.; Tatsumi, T. Activation Energies for the Reaction of Ethoxy Species to Ethene over Zeolites. *J. Phys. Chem. C* **2010**, *114*, 20107−20113.
(34) Kondo, J. N.; Ito, K.; Yoda, E.; Wakabayashi, F.; Domen, K. An Ethoxy Intermediate in Ethanol Dehydration on Brønsted Acid Sites in Zeolite. *J. Phys. Chem. B* **2005**, *109*, 10969−10972.
(35) Clark, J. M.; Nimlos, M. R.; Robichaud, D. J. Bimolecular Decomposition Pathways for Carboxylic Acids of Relevance to Biofuels. *J. Phys. Chem. A* **2015**, *119*, 501−516.
(36) Seshadri, V.; Westmoreland, P. R. Concerted Reactions and Mechanism of Glucose Pyrolysis and Implications for Cellulose Kinetics. *J. Phys. Chem. A* **2012**, *116*, 11997−12013.
(37) Tret'yakov, V. F.; Nhu, C. T. Q.; Tret'yakov, K. V.; Sil'chenkova, O. N.; Matyshak, V. A. Conversion of Ethanol on HZSM-5 Modified Zeolite, According to Data from in Situ Spectrokinetic Studies. *Russ. J. Phys. Chem. A* **2013**, *87*, 941−944.
(38) Laerdahl, J. K.; Uggerud, E. Nucleophilic Identity Substitution Reactions. The Reaction between Water and Protonated Alcohols. *Org. Biomol. Chem.* **2003**, *1*, 2935−2942.
(39) Laerdahl, J. K.; Bache-Andreassen, L.; Uggerud, E. Nucleophilic Identity Substitution Reactions. The Reaction between Ammonia and Protonated Amines. *Org. Biomol. Chem.* **2003**, *1*, 2943−2950.
(40) Boronat, M.; Viruela, P. M.; CORMA, A. Reaction Intermediates in Acid Catalysis by Zeolites: Prediction of the Relative Tendency To Form Alkoxides or Carbocations as a Function of Hydrocarbon Nature and Active Site Structure. *J. Am. Chem. Soc.* **2004**, *126*, 3300−3309.
(41) Haw, J. F. Zeolite Acid Strength and Reaction Mechanisms in Catalysis. *Phys. Chem. Chem. Phys.* **2002**, *4*, 5431−5441.
(42) Horbatenko, Y.; Pérez, J. P.; Hernández, P.; Swart, M.; Solà, M. Reaction Mechanisms for the Formation of Mono- and Dipropylene Glycol from the Propylene Oxide Hydrolysis over ZSM-5 Zeolite. *J. Phys. Chem. C* **2014**, *118*, 21952−21962.
(43) Namuangruk, S. Alkylation of Benzene with Ethylene over Faujasite Zeolite Investigated by the ONIOM Method. *J. Catal.* **2004**, *225*, 523−530.
(44) Pereira, M. S.; da Silva, A. M.; Nascimento, M. A. C. Effect of the Zeolite Cavity on the Mechanism of Dehydrogenation of Light Alkanes over Gallium-Containing Zeolites. *J. Phys. Chem. C* **2011**, *115*, 10104−10113.
(45) Ryder, J. A.; Chakraborty, A. K.; Bell, A. T. Density Functional Theory Study of Proton Mobility in Zeolites: Proton Migration and Hydrogen Exchange in ZSM-5. *J. Phys. Chem. B* **2000**, *104*, 6998−7011.
(46) Nicholas, J. B. Density Functional Theory Studies of Zeolite Structure, Acidity, and Reactivity. *Top. Catal.* **1997**, *4*, 157−171.
(47) van Santen, R. A. Theory of Brønsted Acidity in Zeolites. *Stud. Surf. Sci. Catal.* **1994**, *85*, 273−294.
(48) Joshi, Y. V.; Thomson, K. T. The Roles of Gallium Hydride and Brønsted Acidity in Light Alkane Dehydrogenation Mechanisms using Ga-Exchanged HZSM-5 Catalysts: A DFT Pathway Analysis. *Catal. Today* **2005**, *105*, 106−121.

DOI: 10.1021/jp513024z
J. Phys. Chem. A 2015, 119, 3604−3614

(49) van Santen, R. A.; Rozanska, X.: Theory of Zeolite Catalysis. *In Advances in Chemical Engineering*; Academic Press: New York, 2001; Vol. *28*, pp 399−437.
(50) Dapprich, S.; Komaromi, I.; Byun, K. S.; Morokuma, K.; Frisch, M. J. A New ONIOM Implementation in Gaussian98. Part I. The Calculation of Energies, Gradients, Vibrational Frequencies and Electric Field Derivatives. *J. Mol. Struct. (THEOCHEM)* **1999**, *461*, 1−21.
(51) Fermann, J. T.; Moniz, T.; Kiowski, O.; McIntire, T. J.; Auerbach, S. M.; Vreven, T.; Frisch, M. J. Modeling Proton Transfer in Zeolites: Convergence Behavior of Embedded and Constrained Cluster Calculations. *J. Chem. Theory Comput.* **2005**, *1*, 1232−1239.
(52) Gonzales, N. O.; Bell, A. T.; Chakraborty, A. K. Density Functional Theory Calculations of the Effects of Local Composition and Defect Structure on the Proton Affinity of H−ZSM-5. *J. Phys. Chem. B* **1997**, *101*, 10058−10064.
(53) Lonsinger, S.; Chakraborty, A.; Theodorou, D.; Bell, A. The Effects of Local Structural Relaxation on Aluminum Siting within H-ZSM-5. *Catal. Lett.* **1991**, *11*, 209−217.
(54) Zhao, Y.; Truhlar, D. The M06 Suite of Density Functionals for Main Group Thermochemistry, Thermochemical Kinetics, Noncovalent Interactions, Excited States, and Transition Elements: Two New Functionals and Systematic Testing of Four M06-Class Functionals and 12 Other Functionals. *Theor. Chem. Acc.* **2008**, *120*, 215−241.
(55) Vreven, T.; Morokuma, K. Hybrid Methods: ONIOM(QM:MM) and QM/MM. *Annual Reports in Computational Chemistry*; Elsevier: Amsterdam, 2006; Vol. *2*, Chapter 3 , pp 35−51.
(56) Stewart, J. J. P. Optimization of Parameters for Semiempirical Methods V: Modification of NDDO Approximations and Application to 70 Elements. *J. Mol. Model.* **2007**, *13*, 1173−1213.
(57) Fukui, K. Formulation of the Reaction Coordinate. *J. Phys. Chem.* **1970**, *74*, 4161−4163.
(58) Gonzalez, C.; Schlegel, H. B. An Improved Algorithm for Reaction Path Following. *J. Chem. Phys.* **1989**, *90*, 2154−2161.
(59) Gonzalez, C.; Schlegel, H. B. Reaction Path Following in Mass-Weighted Internal Coordinates. *J. Phys. Chem.* **1990**, *94*, 5523−5527.
(60) Ishida, K.; Morokuma, K.; Komornicki, A. The Intrinsic Reaction Coordinate. An *ab Initio* Calculation for HNC→HCN and $H^-+CH_4 \rightarrow CH_4+H^-$. *J. Chem. Phys.* **1977**, *66*, 2153−2156.
(61) Grimme, S.; Antony, J.; Ehrlich, S.; Krieg, H. A Consistent and Accurate *ab initio* Parametrization of Density Functional Dispersion Correction (DFT-D) for the 94 Elements H-Pu. *J. Chem. Phys.* **2010**, *132*, No. 154104.
(62) Frisch, M. J.; Trucks, G. W.; Schlegel, G. E.; Scuseria, M. A.; Robb, J. R.; Cheeseman, G.; Scalmani, V.; Barone, B.; Mennucci, G. A.; Petersson, H.; et al. *Gaussian 09*, Revision B.01; Gaussian: Wallingford, CT, USA, 2010.
(63) Katada, N.; Suzuki, K.; Noda, T.; Sastre, G.; Niwa, M. Correlation between Bronsted Acid Strength and Local Structure in Zeolites. *J. Phys. Chem. C* **2009**, *113*, 19208−19217.
(64) Shustorovich, E. Chemisorption Theory: In Search of the Elephant. *Acc. Chem. Res.* **1988**, *21*, 183−189.
(65) Sarv, P.; Tuherm, T.; Lippmaa, E.; Keskinen, K.; Root, A. Mobility of the Acidic Proton in Brønsted Sites of H-Y, H-Mordenite, and H-ZSM-5 Zeolites, Studied by High-Temperature ^{1}H MAS NMR. *J. Phys. Chem.* **1995**, *99*, 13763−13768.
(66) Baba, T.; Komatsu, N.; Ono, Y.; Sugisawa, H. Mobility of the Acidic Protons in H-ZSM-5 as Studied by Variable Temperature H-1 MAS NMR. *J. Phys. Chem. B* **1998**, *102*, 804−808.
(67) Hodgson, D.; Zhang, H. Y.; Nimlos, M. R.; McKinnon, J. T. Quantum Chemical and RRKM Investigation of the Elementary Channels of the Reaction C_6H_6 + O (^{3}P). *J. Phys. Chem. A* **2001**, *105*, 4316−4327.
(68) Basch, H.; Hoz, S. *Ab Initio* Study of Hydrogen Abstraction Reactions. *J. Phys. Chem. A* **1997**, *101*, 4416−4431.
(69) Bach, R. D.; Glukhovtsev, M. N.; Gonzalez, C.; Marquez, M.; Estevez, C. M.; Baboul, A. G.; Schlegel, H. B. Nature of the Transition Structure for Alkene Epoxidation by Peroxyformic Acid, Dioxirane, and Dimethyldioxirane: A Comparison of B3LYP Density Functional Theory with Higher Computational Levels. *J. Phys. Chem. A* **1997**, *101*, 6092−6100.
(70) Oie, T.; Topol, I. A.; Burt, S. K. Ab Initio and Density-Functional Studies on Internal Rotation and Corresponding Transition States in Conjugated Molecules. *J. Phys. Chem.* **1995**, *99*, 905−915.
(71) Dobbs, K. D.; Dixon, D. A. Ab Initio Prediction of the Activation Energy for the Abstraction of a Hydrogen Atom from Methane by Chlorine Atom. *J. Phys. Chem.* **1994**, *98*, 12584−12589.
(72) Hasted, J. B. Liquid Water: Dielectric Properties. *Water: A Comprehensive Treatise*; Plenum Press: New York, 1972; Vol. *1*.

DOI: 10.1021/jp513024z
J. Phys. Chem. A 2015, 119, 3604−3614